Stability Map for Nanocrystalline and Amorphous Materials

Shailendra P. Joshi* and K. T. Ramesh†

Department of Mechanical Engineering, The Johns Hopkins University, 3400 North Charles Street, Baltimore, Maryland 21218, USA

(Received 28 March 2008; published 9 July 2008)

We present a stability map which predicts the domains of shear instability due to grain rotation in nanocrystalline materials. The onset of this mode of instability is influenced by grain-size-dependent mechanisms and the length-scale of intergranular interaction. The map shows the grain size regimes that are inherently susceptible to this mode for a range of materials. In the amorphous limit, the model predicts embryonic nuclei sizes of about 10–50 nm, which agrees well with the shear band thicknesses for many metallic glasses.

DOI: 10.1103/PhysRevLett.101.025501 PACS numbers: 62.25.−g, 61.46.−w

Rotational deformation mechanisms are ubiquitous in many materials ranging from nanocrystalline (NC) metals [1–4] to geological and granular media [5,6] and even in amorphous solids [7,8]. These mechanisms have important implications on the overall material response and invoke modes of macroscopic deformation that are often spatially inhomogeneous. For example, grain rolling has been shown to be a critical mode of deformation that leads to macroscopic shear bands in granular materials [9,10]. In amorphous metals the flipping of so-called shear transformation zones (STZs) may cause local softening that drives the shear localization process [11]. In NC metals, grain rotation coupled with grain boundary (GB) mechanisms [1,12] may lead to conflicting consequences such as enhanced ductility due to grain growth [13,14] or localized deformation through shear banding [15]. The implications of this deformation mechanism for instability in the truly NC regime ($d \ll 100$ nm) are of great interest as many NC metals lack stable plastic response [16]. How susceptible is a material to strain localization due to grain rotation for a given grain size? Is there a range of grain sizes over which a material will exhibit this instability given its crystalline structure? How does the transition from intragranular (crystalline) to intergranular (GB) mechanisms influence the grain rotation behavior in the NC regime of grain sizes? What are the critical perturbation (defect nuclei) length-scales that may lead to runaway instabilities at grain sizes approaching the amorphous limit? In this Letter, we lay out a map that characterizes the inherent susceptibility of materials to shear instability driven by the grain-size-dependent rotational deformation mode. The stability problem is investigated through a first-order perturbation analysis of a nonlocal continuum model for the grain rotation driven shear instability [17]. The nonlocal character of this model resides in an evolution equation for an internal variable (ϕ) that represents the grain rotation

$$\dot{\phi} = \psi\dot{\gamma}_p + D_r\frac{\partial^2\phi}{\partial X^2}. \tag{1}$$

In Eq. (1), the internal variable $\phi(t)$ is defined by the number fraction $\phi(t) = N_s(t)/N_b$, with $N_s(t)$ being the number of grains at time t that have their plastically softest (s) crystallographic orientations aligned with the shearing direction in a representative volume element (RVE) containing a total number of grains N_b. With incremental loading some fraction of the current unfavorably oriented grains in an RVE rotate and align their s-orientations along the shearing direction. The rotational diffusion coefficient $D_r(= \mu d^2/(2-\nu)j\eta_{\text{eff}})$ describes the intergranular interaction due to grain rotation; here, μ is the elastic shear modulus, d is the mean grain size, ν is the Poisson's ratio. The effective viscosity (η_{eff}) describes the resistance of the accommodating region with contributions from the bulk crystalline plasticity (η_{bulk}) and boundary (η_b) mechanisms [17] and is given as $(\eta_{\text{eff}})^{-1} = (\eta_{\text{bulk}})^{-1} + (\eta_b)^{-1}$, where $\eta_{\text{bulk}} = (\tau_{s0}/\dot{\gamma}_0)$ and $\eta_b = (k_B T d^3/64\delta\Omega D_{\text{gb}})$ [18], k_B being the Boltzmann constant, T the temperature, δ the GB thickness (assumed 1 nm) [18], Ω the atomic volume, and D_{gb} the GB diffusion coefficient. ψ is a fabric factor that incorporates the initial texture and grain size effects [i.e., $\psi = f(\phi)g(d)$]. The local plastic shear strain rate $\dot{\gamma}_p$ in Eq. (1) is defined using the constitutive law $\dot{\gamma}_p = \dot{\gamma}_0\langle\{\tau\tau_0^{-1}(1-\bar{c}\phi)^{-1}\}^{1/m} - 1\rangle$, where τ is the average shear stress, and τ_0, γ_0, $\dot{\gamma}_0$ and m represent the grain-size-dependent shear yield strength, the corresponding yield strain, the characteristic strain rate, material strain rate sensitivity, respectively; $(1-\bar{c}\phi)$ represents a monotonically softening response due to grain rotation. The anisotropy parameter $\bar{c}(= 1 - \tau_{s0}/\tau_{h0})$ depends on the single crystal flow strengths in the softest (τ_{s0}) and hardest (τ_{h0}) orientations.

The rotation of a single grain is accommodated through rotation and slip in the adjacent grains over an ensemble with a characteristic length L [Fig. 1(a)], and the rotational influence parameter $j(= L/d)$ is (along a radial direction) the number of grains in this ensemble participating in the dissipative accommodation process. If L is fixed, then j increases as the grain size reduces, and this is reasonable for ultrafine-grained (ufg) materials (100 nm $< d <$ 1 μm) where the largest grains will deform plastically rather than rotate. However, in the truly NC regime, the conventional modes of plastic deformation such as the

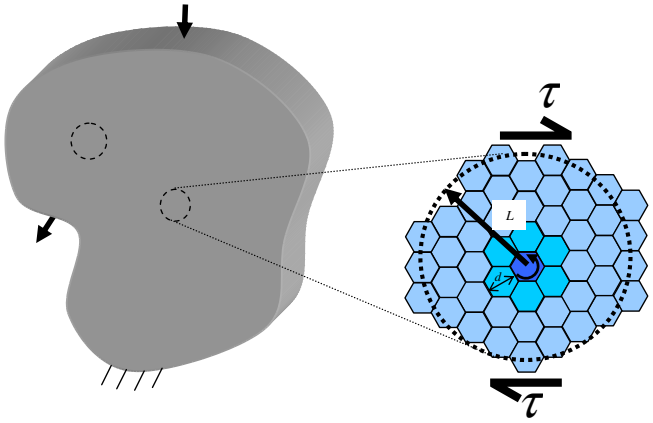

FIG. 1 (color online). Schematic of the rotational accommodation length scale (L or L_g) in a material continuum.

crystallographic slip are greatly inhibited. In the limiting case of purely elastic grains, one would expect that a grain that is a sufficient *number* of grains (rather than a sufficient distance) away from the rotating grain would not perceive the rotation. That is, for elastic granular solids one expects a rotational accommodation distance determined by a finite number of grains, so that j is fixed (say j_g) rather than L. A consequence is that smaller grain sizes will imply smaller accommodation lengths $L_g = j_g d$. This is consistent with observations in some elastic granular solids where the dissipative intergranular interactions set up the shear band thicknesses of the order of tens of grain diameters [19]. At the other extreme, i.e., for coarse-grained metals ($d\sim$ several microns) where crystallographic slip dominates the problem, the rotational mechanism may not exist at all; thus, L must have an upper limit (assumed 1 μm here). Thus, for ufg materials (100 nm $\leq d \leq$ 1 μm) and coarser grained materials, we set the rotational accommodation length scale to the fixed value $L = 1$ μm, and the rotational influence parameter j will vary with the grain size d. For NC materials (1 nm $< d \leq$ 100 nm) we set the accommodation number of grains to the fixed value $j_g = 10$ (based on the elastic granular solid approximation, where intergranular interaction distances are believed to be about 10 grain diameters), and the rotational accommodation distance L_g will vary with grain size d.

For simplicity we consider a one-dimensional system comprising an NC material specimen of unit thickness deformed in simple shear at a constant rate ($\dot{\gamma}$) in the X-direction (normal to the thickness). We set up the governing equations in terms of normalized variables for position ($\hat{X} = X/L$), shear stress ($\hat{\tau} = \tau m/\tau_{s0}\bar{c}$) and time ($\hat{t} = \dot{\gamma}_0 t$). Using these scaled variables, the equilibrium condition is ($\partial\hat{\tau}/\partial\hat{X} = 0$), and the elastic relation is $\hat{\tau} = \mathbf{M}^{-1}(\hat{\dot{\gamma}} - \hat{\dot{\gamma}}_p)$, where $\mathbf{M}(= \tau_{s0}\bar{c}/\mu\text{m})$ is a strength index that will be utilized later in constructing the stability map. The normalized evolution equation (Eq. (1)) is $\hat{\dot{\phi}} = \psi\hat{\dot{\gamma}}_p + \frac{D_r}{\dot{\gamma}_0 L^2}\frac{\partial^2\phi}{\partial\hat{X}^2}$, where $\hat{\dot{\gamma}}_p$ is the scaled viscoplastic shear strain rate.

We analyze the stability of the governing equations using linear perturbation analysis and therefore restrict our attention to early times, i.e., onset of instability. With $\hat{\tau}$ required to be homogeneous (the equilibrium condition) the stability of deformation is investigated by perturbing the plastic strain γ_p and the internal variable ϕ from their homogeneous solutions: $\tilde{\phi} = \phi^h + \delta\phi(\hat{t})\sin k\hat{X}$ and $\tilde{\gamma}_p = \gamma_p^h + \delta\gamma_p(\hat{t})\sin k\hat{X}$, k being the nondimensional wave number of perturbation. The normalized temporal components of perturbations $[(\delta\phi(\hat{t}), \delta\gamma_p(\hat{t})]$ are assumed small with respect to their homogeneous solutions (ϕ^h, γ_p^h). Substituting the perturbed solutions in the normalized evolution equation $(\hat{\dot{\phi}})$ and retaining only the first-order terms we find that the perturbations will grow if $\frac{\partial\hat{\dot{\gamma}}_p^h}{\partial\phi} > (\frac{k^2 D_r}{\psi\dot{\gamma}_0 L^2})$. Letting $\phi^h = 0$, the constitutive law together with $\tilde{\phi}$ and $\tilde{\gamma}_p$ gives $\frac{\partial\hat{\dot{\gamma}}_p^h}{\partial\phi} \approx (\frac{\bar{c}}{m})\hat{\dot{\gamma}}_p^h$. Then, the critical wavelength λ_{crit} that may lead to runaway instability is

$$\lambda_{\text{crit}} = \left[\left(\frac{\dot{\gamma}_0\hat{\dot{\gamma}}_p^h\psi}{D_r}\left\{\frac{\bar{c}}{m}\right\}\right)^{1/2}\right]^{-1} = \left[\frac{\mathbf{M}}{(2-\nu)\psi\hat{\dot{\gamma}}_p^h}\left(\frac{d^2}{j}\right)\left(\frac{\eta_{\text{bulk}}}{\eta_{\text{eff}}}\right)\right]^{1/2}. \quad (2)$$

Note that Eq. (2) admits general grain size distributions through ψ; here for simplicity we ignore this variation and associate λ_{crit} with a unique microstructural size, d. Equation (2) shows that materials with high crystallographic plastic anisotropy and low rate sensitivity are generally susceptible to instability. The grain size dependence of λ_{crit} appears through D_r. Note that when $(\lambda_{\text{crit}}/d) \approx 1$ the material is inherently unstable in that this perturbation necessarily exists in the material; $(\lambda_{\text{crit}}/d) < 1$ is mathematically possible but not physically meaningful unless grain size distributions are included. For most materials the fabric factor (ψ) will range between 1–10. Setting $\psi = 10$ and $\hat{\dot{\gamma}}_p^h = 1$ (with $\dot{\gamma}_0 = 5 \times 10^{-4}$ s^{-1}), we examine the dependence of λ_{crit} on grain size. Figure 2 shows the $\lambda_{\text{crit}} - d$ relationship for three materials (Table I), bcc-Fe, fcc-Cu, and fcc-Al. For all these materials, there are in general three regimes in this log-log plot as the grain size is decreased. In the first regime ($d \geq$ 100 nm), λ_{crit} decreases with decreasing grain size, the maximum number of participating grains is determined by fixed L, and η_{bulk} is the rate limiting process. This rate limiting process continues to dominate the second regime (100 nm $\geq d \geq$ 10 nm), which is governed by the limited number of participating grains (j_g), and λ_{crit} decreases with a different slope. In the third regime ($d <$ 10 nm) λ_{crit} increases as the grain size decreases. This is because the dominant rate limiting process changes from being intragranular (η_{bulk} to GB driven (η_b). The region below the line $\lambda_{\text{crit}} = d$ in Fig. 2 is the inherently unstable domain. As an example, for 300 nm grain size Fe, λ_{crit} is approximately equal to the grain size. A similar calculation for Cu yields $\lambda_{\text{crit}} \sim 440$ nm, which is somewhat higher

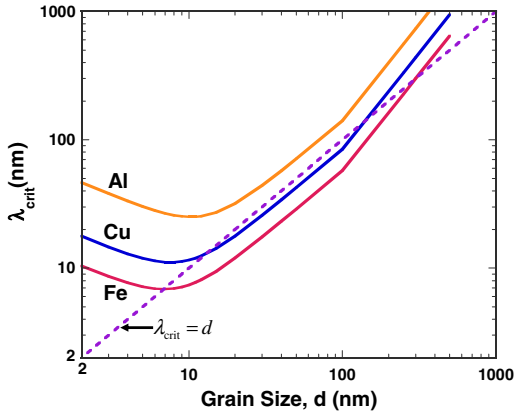

FIG. 2 (color online). Critical wavelength (λ_{crit}) as a function of grain size for three materials (log-log plot). We set $j_g = 10$ below $d = 100$ nm. For 100 nm $< d \leq 1$ μm, $L = 1$ μm and $j = L/d$.

than the corresponding grain size. Consequently, the Fe is inherently susceptible to instability over a larger range of grain sizes than the Cu. For some materials the entire curve will be above the inherent instability line (e.g., the Al-curve in Fig. 2). The grain size range over which a material is inherently unstable (if at all) is intimately tied to its elastic properties, plastic anisotropy, and the strain rate sensitivity.

An interesting result follows when we consider the onset of instability for grain sizes approaching the GB thickness (an effective definition of being amorphous). For $d =$ 2 nm (the amorphous limit), the embryonic nuclei that may cause shear instability are found to be $\lambda_{\text{crit}} \approx 10$ nm for Fe, ≈ 18 nm for Cu and ≈ 45 nm for Al. These embryonic nuclei sizes depend on the elastic properties, which may be modified by the properties of the GB phase [20]. The predicted nucleus size of 10–50 nm is within the shear band thickness range for metallic glasses [19,21,22]. However, the constitutive description does not include pressure dependence of the plastic flow, which may be important for metals with grain sizes approaching amorphous limits [23,24].

This stability analysis allows one to probe the likelihood of instability in the materials and microstructure space. Figure 3 presents a stability map where the ordinate is the previously defined strength index **M** that enables one to compare different materials while the abscissa is the grain size. The curve is the locus of points satisfying the inherent instability criterion ($\lambda_{\text{crit}} = d$). If the point representing a given material and grain size lies in the saddle (the blue region), then the material is inherently susceptible to the rotational mechanism of shear instability. In general, materials with low strength indices show susceptibility over a smaller range of grain sizes compared to those with higher strength indices. Thus, the Fe is inherently susceptible to rotational instability over a larger grain size range than the Cu, while Al does not exhibit any inherent instability. This prediction is qualitatively consistent with the available data on NC-Fe [15], NC-Cu [25], and NC-Al [13,26]. Note that a combination of $\mathbf{M} - d$ lying outside the inherent instability region (the orange region) does not unambiguously guarantee a stable response, as instability can still occur at larger perturbation wavelengths but such a material would not be inherently unstable. Such maps may provide useful guidelines to determine the probability of a material being unstable to this softening mechanism for a range of defect wavelengths.

We comment here on the nature of the rotational inelastic mechanism in other material systems and the applicability of this model in predicting the resulting shear instabilities. A common feature in the exemplar cases of the crystalline, granular, and amorphous materials is that there is an underlying microstructural rotational unit (the μ-unit) that sets up a wavelength that governs the nucleation and growth of shear bands. In metals and granular materials this μ-unit is the grain size whereas in amorphous metals it is the size of an STZ. During the rotational deformation process a μ-unit will interact with other μ-units through contact (kinematics) and/or continuum stress fields (dynamics), thereby giving a nonlocal character. Given that these basic building blocks are embedded in our "grain" rotation model, it is possible to apply this analogy to a variety of materials by generalizing the internal variable ϕ as a homogenized description of the relevant μ-unit. Besides this, two important changes are needed depending on the class of materials that are being investigated. First, the inelastic response assumed for the crystalline materials needs to be replaced by appropriate constitutive laws (e.g., pressure dependent plasticity in amorphous metals). Second, suitable softening mechanisms need to be incorporated within the constitutive framework through the evolution law for ϕ. For example, in granular materials the source term (first term on the right side of Eq. (1)) may represent the local material spin (ω) as a scaled function of the local shear rate ($\dot{\gamma}$) causing the force chains to buckle [10]; the anisotropy parameter ($\bar{c}$) may resemble the geometric anisotropy (grain size and shape variation) that controls the degree of softening, while the variations in rolling resistances may be accounted for

TABLE I. Default material parameters for instability calculations.

	μ (GPa)	ν	$\bar{c}$	m	τ_{s0} (MPa)	Ω (m^3)	D_{gb} (m^2/s)	**M**
Fe	76	0.29	0.07	0.005	100	2.13×10^{-29}	1.0×10^{-20}	0.018
Cu	48	0.34	0.030	0.030	81	1.30×10^{-29}	2.6×10^{-20}	0.0085
Al	26	0.30	0.044	0.044	29	8.18×10^{-30}	2.9×10^{-19}	0.003

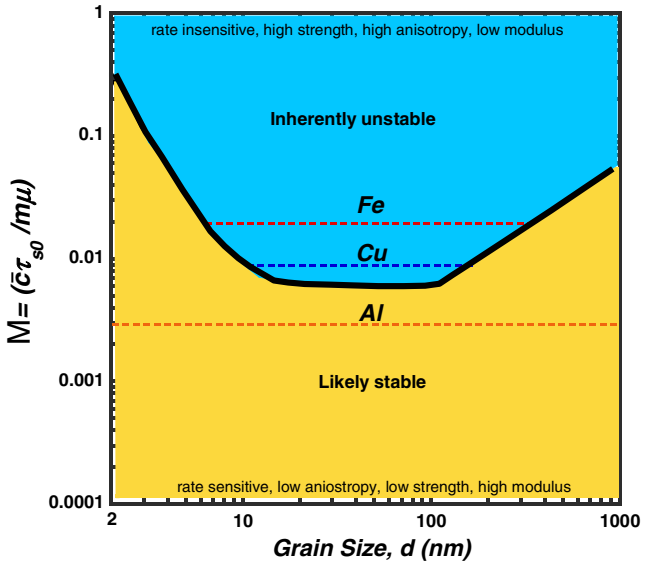

FIG. 3 (color online). A map showing inherent instability ($\lambda_{\mathrm{crit}} = d$) bounds for different materials.

through D_r. For amorphous metals, the evolution of ϕ will describe the evolution of STZ number density. The relevant softening mechanism is that of the local reduction in mass density (and therefore, an increase in free volume) due to resulting dilation. We note the qualitative similarity between Eq. (1) and a free volume evolution equation for metallic glasses [27].

This one-dimensional model can be generalized for implementation in a 3D computational framework. The extension of the governing equations is straightforward. The constitutive description can be generalized easily using linear elasticity theory and identifying the shear stress and plastic shear strain rate in this paper with the effective stress ($\sqrt{J_2}$) ($J_2 = \frac{1}{2} S_{ij} S_{ij} = Y^2$, where S_{ij} are components of deviatoric stress and Y is the yield strength) and the effective plastic strain rate ($\dot{e}^p = \sqrt{\frac{2}{3}(\mathbf{d}^p{:}\mathbf{d}^p)}$) derivable from the full stress and rate of deformation ($\mathbf{d}^p$) tensors. In general, a tensorial description for the orientation states of the internal variable [28] may be necessary. Langer and co-workers [8,11,29] have developed elegant concepts to address these issues in amorphous solids, which could form a basis for generalization of our approach. A more comprehensive treatment for the evolution law should also account for anisotropy of intergranular interaction in 3D, for example, through anisotropic D_r (and L). In the isotropic 3D idealization of the evolution law, to first order the critical nucleus sizes will remain similar. The real difficulty is in the propagation and intersection of shear bands, important in three dimensions, but the physics of which are not understood. We will address these issues in a future work.

The key new results—identification of the strength metric for susceptibility, and the development of the stability map—have not been available before, and have potential use in a variety of classes of materials.

The authors are grateful for the financial support received from the Army Research Laboratory (No. W911NF-06-2-0006).

*Present address: Department of Mechanical Engineering, National University of Singapore, Singapore.
†Corresponding author.
ramesh@jhu.edu

[1] J. W. Cahn and J. E. Taylor, Acta Mater. **52**, 4887 (2004).
[2] A. J. Haslam, D. Moldovan, V. Yamakov, and D. Wolf *et al.*, Acta Mater. **51**, 2097 (2003).
[3] M. Murayama, J. M. Howe, H. Hidaka, and S. Takaki, Science **295**, 2433 (2002).
[4] M. Upmanyu, D. J. Srolovitz, A. E. Lobkovsky, and J. A. Warren *et al.*, Acta Mater. **54**, 1707 (2006).
[5] A. Aydina, R. I. Borja, and P. Eichhubl, J. Struct. Geol. **28**, 83 (2006).
[6] D. M. Mueth, G. F. Debregeas, G. S. Karczmar, and P. J. Eng *et al.*, Nature (London) **406**, 385 (2000).
[7] A. S. Argon, Acta Metall. **27**, 47 (1979).
[8] M. L. Falk and J. S. Langer, Phys. Rev. E **57**, 7192 (1998).
[9] N. Hu and J. F. Molinari, J. Mech. Phys. Solids **52**, 499 (2004).
[10] A. L. Rechenmacher, J. Mech. Phys. Solids **54**, 22 (2006).
[11] J. S. Langer, Phys. Rev. E **64**, 011504 (2001).
[12] M. Y. Gutkin and I. A. Ovid'ko, Appl. Phys. Lett. **87**, 251916 (2005).
[13] D. Gianola, S. V. Petegem, M. Legros, and S. Brandstetter *et al.*, Acta Mater. **54**, 2253 (2006).
[14] D. S. Gianola, C. Eberl, X. M. Cheng, and K. J. Hemker, Adv. Mater. **20**, 303 (2008).
[15] D. Jia, K. T. Ramesh, and E. Ma, Acta Mater. **51**, 3495 (2003).
[16] C. C. Koch, Scr. Mater. **49**, 657 (2003).
[17] S. P. Joshi and K. T. Ramesh, Acta Mater. **56**, 282 (2008).
[18] M. A. Meyers, A. Mishra, and D. J. Benson, Prog. Mater. Sci. **51**, 427 (2006).
[19] Y. Zhang and A. L. Greer, Appl. Phys. Lett. **89**, 071907 (2006).
[20] A. Latapie and D. Farkas, Scr. Mater. **48**, 611 (2003).
[21] M. Chen, A. Inoue, W. Zhang, and T. Sakurai, Phys. Rev. Lett. **96**, 245502 (2006).
[22] F. Shimizu, S. Ogata, and J. Li, Acta Mater. **54**, 4293 (2006).
[23] A. C. Lund, T. G. Nieh, and C. A. Schuh, Phys. Rev. B **69**, 012101 (2004).
[24] C. A. Schuh, T. C. Hufnagel, and U. Ramamurty, Acta Mater. **55**, 4067 (2007).
[25] S. Cheng, E. Ma, Y. M. Wang, and L. J. Kecskes *et al.*, Acta Mater. **53**, 1521 (2005).
[26] P. L. Sun, E. K. Cerreta, G. T. Gray, and J. F. Bingert, Metall. Mater. Trans. A **37**, 2983 (2006).
[27] R. Huang, Z. Suo, J. H. Prevost, and W. D. Nix, J. Mech. Phys. Solids **50**, 1011 (2002).
[28] L. Pechenik, Phys. Rev. E **72**, 021507 (2005).
[29] J. S. Langer and L. Pechenik, Phys. Rev. E **68**, 061507 (2003).